Biochemistry

pubs.acs.org/biochemistry Article

Elucidation of pH-Induced Protein Structural Changes: A Combined 2D IR and Computational Approach

Shivshankar Kore, Samadhan H. Deshmukh, Sushil S. Sakpal, Srijan Chatterjee, Atanu Das,* and Sayan Bagchi*

Cite This: *Biochemistry* 2023, 62, 451−461 Read Online

ACCESS | Metrics & More | Article Recommendations | Supporting Information

ABSTRACT: The acid−base behavior of amino acids plays critical roles in several biochemical processes. Depending on the interactions with the protein environment, the pK_a values of these amino acids shift from their respective solution values. As the side chains interact with the polypeptide backbone, a pH-induced change in the protonation state of aspartic and glutamic acids might significantly influence the structure and stability of a protein. In this work, we have combined two-dimensional infrared spectroscopy and molecular dynamics simulations to elucidate the pH-induced structural changes in an antimicrobial enzyme, lysozyme, over a wide range of pH. Simultaneous measurements of the carbonyl signals arising from the backbone and the acidic side chains provide detailed information about the pH dependence of the local and global structural features. An excellent agreement between the experimental and the computational results allowed us to obtain a residue-specific molecular understanding. Although lysozyme retains the helical structure for the entire pH range, one distinct loop region (residues 65−75) undergoes local structural deformation at low pH. Interestingly, combining our experiments and simulations, we have identified the aspartic acid residues in lysozyme, which are influenced the most/least by pH modulation.

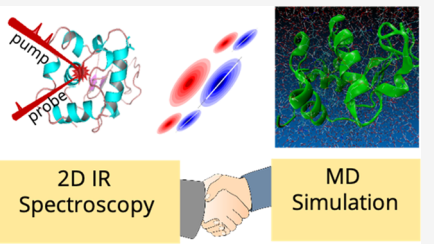

INTRODUCTION

Vibrational modes of the peptide units are sensitive indicators of the protein secondary structures. The protein conformations dictate the electrostatic interactions (couplings) between individual amide carbonyls (C═O) along the polypeptide backbone. These interactions govern the essential aspects of the structural topology in proteins and get manifested in the amide-I frequencies of the infrared (IR) spectrum. The amide-I mode in proteins is highly degenerate and delocalized with sufficient range to sense the secondary structure.[1−5] IR spectroscopy, intrinsic to all proteins, is an appealing method for the identification of protein conformations and the mesoscopic structure.

Despite the potential advantages, the large spectral width of the amide-I spectrum makes the application of such structural correlations extremely difficult.[6] Therefore, the traditional protein IR spectroscopy is limited as a qualitative tool.[7] On the other hand, two-dimensional infrared (2D IR) spectroscopy spreads the spectral information into two axes and deciphers the overlapping contributions to the broad peak. 2D IR permits the direct experimental examination of the electrostatic couplings between amide units through the formation of cross-peaks, thereby providing a spectroscopic route toward the structural interpretations of the proteins.[8−10]

In addition to the polypeptide backbone, the side chains interacting with the backbone have a significant influence on the protein structure, solubility, and stability.[11,12] It has been previously reported that the acidic side chains of aspartic (Asp) and glutamic (Glu) acids are coupled to the amide-I modes.[13] As the protonation state of these side chains dictates the interactions, any change in the protonation state can affect the protein structures and make the stability of the proteins pH-dependent. The pK_a values of Asp and Glu in proteins, greatly influenced by the local environment, can differ significantly from those measured for individual amino acids. For example, while the average pK_a value measured in proteins for Asp is 3.5, values ranging from 0.5 to 9.2 have been reported for this residue.[11] The pK_a values are often seen to be hugely altered in the enzyme active sites.[14] The factors influencing the pK_a values are of intense biochemical interest.

The carboxylic acid/carboxylate C═O vibrations of Asp and Glu have frequencies close to that of the amide-I mode. Experimental and theoretical studies of several acids have reported the pH dependence of these IR absorptions.[15−20] At low pH (<pK_a), one absorption band is observed in the 1700−1730 cm^{-1} range, corresponding to the protonated side chain (−COOH). At high pH (> pK_a), COOH gets deprotonated to form COO$^-$ and the IR absorption band is observed in the frequency range of 1550−1590 cm^{-1}, corresponding to the

Received: November 3, 2022
Published: December 27, 2022

https://doi.org/10.1021/acs.biochem.2c00626
Biochemistry 2023, 62, 451−461

asymmetric COO^- vibration. The spectrally distinguishable C═O frequencies of the carboxylate and carboxylic acid, when studied in tandem with the amide-I peaks, make them useful vibrational probes to study the effect of pH on the protein structure.

The intrinsically broad bandwidth of the 2D IR method allows simultaneous measurement of the C═O signals arising from the polypeptide backbone and the acidic side chains, thereby providing detailed information about the pH dependence of the local (acidic side chains) and global structural features (amide-I). The carboxylic acid/carboxylate bands being naturally occurring spectroscopic markers of the protonation state, pH-selective 2D IR experiments can further shed light on the approximate pK_a values of these groups in a protein environment. In addition, the presence of cross-peaks between the side chain C═O and the amide-I mode can indicate the extent of couplings between the side chains and the backbone amides. A detailed 2D IR study can provide a plethora of information regarding how a change in the solution pH can modify the protonation state, leading to conformational changes in the protein. 2D IR results can be directly compared with molecular dynamics (MD) simulations. A general agreement of the experimental and computational results would allow us to obtain a residue-specific molecular picture.

In this work, we have combined IR absorption spectroscopy, 2D IR spectroscopy, and MD simulations on an antimicrobial enzyme, hen egg-white lysozyme, to extensively study the pH-induced structural changes. Lysozyme is predominantly an α-helical protein consisting of 129 amino acid residues, of which nine have acidic side chains (seven Asp and two Glu). We have chosen lysozyme because the enzyme has been previously categorized as a type III protein, which shows no significant change in the secondary structure at extremely low pH.[21] Our results demonstrate the protonation/deprotonation of Asp and Glu with changes in pH. 2D IR spectra show that these side chains are coupled to the backbone, manifested as cross-peaks. 2D IR polarization difference spectroscopy further indicates that the α-helices remain more or less intact in alkaline (pH 9), neutral (pH 7), and acidic (pH 2) conditions. The invariance of the α-helical content is in excellent agreement with the results obtained from MD simulations and previously reported acid titration experiments.[21] Further, simulation results indicate subtle pH-dependent structural changes in the specific segment (N65-L75) of a very long loop (G54-P78, connecting β2 and α3) of the protein. Interestingly, constant pH MD simulations have indicated large differences in the pK_a values of the acidic side chains in lysozyme, which agrees with the 2D IR results.[22] Detailed inspection shows that Asp52 has the least solvent-accessible surface area (SASA), whereas Asp66 shows the most significant change in solvent exposure when the pH is varied from 2 to 9. We have successfully demonstrated that a combination of MD simulations and 2D IR spectroscopy can predict the pH-induced subtle changes in protein structures.

MATERIALS AND METHODS

Sample Preparation. The hen egg-white lysozyme was directly purchased from Sigma-Aldrich and used without further purification. Buffer solutions of pH ∼2, pH ∼7, and pH ∼9 were prepared with HCl−KCl buffer, sodium phosphate buffer, and Tris-HCl buffer, respectively. The pH of the same was measured using a pH meter. A protein solution of 2 mM was prepared for the experiments. All of the buffers were prepared in D_2O to avoid absorption in the amide- I frequency region.

FTIR Measurements. A Bruker Vertex 70 Fourier transform infrared spectroscopy (FTIR) spectrometer with 2 cm^{-1} resolution was used to measure the IR absorption spectra at 22 °C. For each sample, ∼100 μL of the sample solution was loaded into a demountable cell, consisting of two demountable CaF_2 windows separated by a mylar spacer of 56 μm thickness.

CD Spectroscopy. The circular dichroism (CD) measurements were performed on a Jasco J-815 spectropolarimeter. The instrument settings used for collecting the data were as follows: data integration time, −4 s; bandwidth, −2 nm; data pitch, −1 nm; scan speed, −50 nm/min. Each spectrum was an average of five accumulations. Far-ultraviolet (UV) spectra were collected in the wavelength range of 200−250 nm with a cuvette length of 0.1 cm. The protein concentration was ∼10 μM. Same settings was used for collecting the spectra of buffers, and the buffer spectrum was later subtracted from the respective lysozyme solution.

2D IR Measurements. A detailed description of the 2D IR setup was described previously.[23] In brief, a Ti:sapphire regenerative amplifier was used to pump an optical parametric amplifier (OPA). The signal and idler beams, focused at the difference frequency generation ($AgGaS_2$) crystal, produced IR pulses. This ultrashort (∼50 fs) IR pulse has been directed to the 2D IR spectrometer (PhaseTech), where the pulse was split into a strong pump (80%) and a weak probe (20%) beam. The pump pulse was passed through a pulse shaper to generate a collinear pair of compressed pump pulses with variable delays (τ) that were scanned to generate the pump axis (excitation frequencies) of the 2D IR spectra. Parabolic mirrors focused the pump and probe pulses at the sample position. At zero temporal delay between the pump and the probe pulses (waiting time, T_w), τ was scanned to generate the 2D IR signal. The signal was dispersed with a monochromator and detected on a liquid nitrogen-cooled IR array detector (InfraRed Associates). All 2D IR spectra have been collected at 22 °C temperature. The sample cells for 2D IR experiments have been prepared in the same manner as that for the IR absorption experiments except that the spacer used here was of 25 μm thickness, to decrease the background absorption from the aqueous buffer.

Polarization-selective 2D IR experiments were performed in the parallel ⟨*XXXX*⟩ and perpendicular ⟨*XXYY*⟩ polarization conditions, where the polarization of the pump beam was either parallel or perpendicular with respect to that of the probe beam. Pump polarization before the sample was controlled using the combination of a half-wave plate and a polarizer. The 2D IR spectra for all of the solution conditions were collected at T_w = 0 ps in both the polarization conditions.

Molecular Dynamics Simulation. Molecular dynamics simulations were performed using the GROMACS software package, version 5.1.4.[24] Parameters for the protein were taken from the CHARMM27 parameter set.[25] The experimentally determined structure of lysozyme (Protein Data Bank accession code: 1AKI) was taken as the initial structure for the simulation.[26] Three different sets of simulations were performed to identify the effect of pH on lysozyme—acidic (pH 2), neutral/physiological (pH 7), and alkaline (pH 9). At any given pH, the protonation states of the Asp and Glu were determined from previously reported pK_a values obtained from the Amber tutorial on constant pH molecular dynamics simulations of lysozyme (https://ambermd.org/tutorials/

https://doi.org/10.1021/acs.biochem.2c00626
Biochemistry 2023, 62, 451−461

advanced/tutorial18/). The −COO side chains of the Asp and the Glu residues were selectively kept protonated and deprotonated (Table S1) to mimic the low and high pH conditions. Specifically, Asp48 and Asp52 were kept deprotonated for simulations mimicking pH 2 and Glu35 was kept protonated at pH 7. The experimental value of pK_a = 2 is chosen for Asp66 and its side chain is kept in the protonated form for the pH 2 simulation.[27] This selective (de)protonation of the −COO groups was performed to complement the IR spectroscopy technique utilized in this work, where the −COO(H) stretching acts as a structural probe for the protein.

Lysozyme was solvated with TIP3P water molecules in a cubic box so that the minimal distance of the protein from any edge of the cubic box was at least 10 Å, which gave us a box dimension of 70.1 × 70.1 × 70.1 Å^3. Electroneutrality of the system was achieved by adding counter ions (Cl^-) using the genion module of GROMACS. Water molecules were randomly replaced with Cl^- ions at favorable sites determined by computing the electrostatic potential at the insertion site. This procedure gave us the final composition of the protein, which was subjected to the steepest descent energy minimization to arrive at conformations with no steric clashes. Each of these minimized conformations was equilibrated in two phases, with position restraints applied to all of the heavy atoms throughout the simulations. Using the modified Berendsen weak coupling method, the first phase of equilibration involved simulating each system for 500 ps under a constant volume (NVT) ensemble at 300 K.[28] The position of the protein was restrained near the center of the cubic box with a force constant of 1000 kJ mol^{-1} nm^{-2}. Following NVT equilibration, 500 ps of constant pressure (NPT) equilibration was performed, where pressure was maintained isotropically at 1.0 bar using the Parrinello−Rahman barostat;[29] the protein position was again kept near the center of the cubic box using a force constant of 1000 kJ mol^{-1} nm^{-2}. In terms of varying pH, each of the three different protein systems was then used to perform a set of three independent 1 μs of NPT (P = 1 bar and T = 300 K) simulations without any constraints (production MD runs) leading to a total of 3 μs of simulated trajectories at each pH (a total of 9 μs of simulation). The following parameters were employed in the simulations: (1) the integration time step was 2 fs; (2) snapshots of the trajectories were stored after every 20 ps; and (3) the nonbonded interactions list was updated after every 10 steps. The LINCS algorithm[30] was used to constrain all bonds that contained a hydrogen atom to their precise length, with a warning angle of 30°. The protein, waters, and Cl^- ions were coupled to separate temperature baths with a relaxation constant of 0.1 ps and separate constant pressure barostats using Parrinello−Rahman scaling with a relaxation constant of 1.0 ps, and isothermal compressibility of 4.5 × 10^{-5} bar^{-1}. All simulations employed periodic boundary conditions with the standard minimum image convention in all three directions. Long-range electrostatics was treated with the particle mesh Ewald method[31] with a real-space cutoff at 9 Å. The cutoff used for Lennard-Jones interactions was 9 Å with 1.2 Å Fourier spacing.

RESULTS AND DISCUSSION

FTIR Spectra. FTIR spectra of lysozyme in the 1500−1750 cm^{-1} region, shown in Figure 1 as a function of pH, show broad amide-I peaks in the 1600−1690 cm^{-1} region. The amide-I peaks, centered at ∼1650 cm^{-1}, are almost identical at pH 7 and 9. At pH 2, the peak shows a 3 cm^{-1} blue shift and broadens at the high-frequency side. The broadening of the peak indicates a larger inhomogeneous distribution of the protein conformations, which can plausibly arise from a less compact ensemble. Although amide-I transitions are primarily utilized to study protein structures, the other transitions seen in Figure 1 can act as complementary vibrational markers to demonstrate the effect of pH on lysozyme.[13]

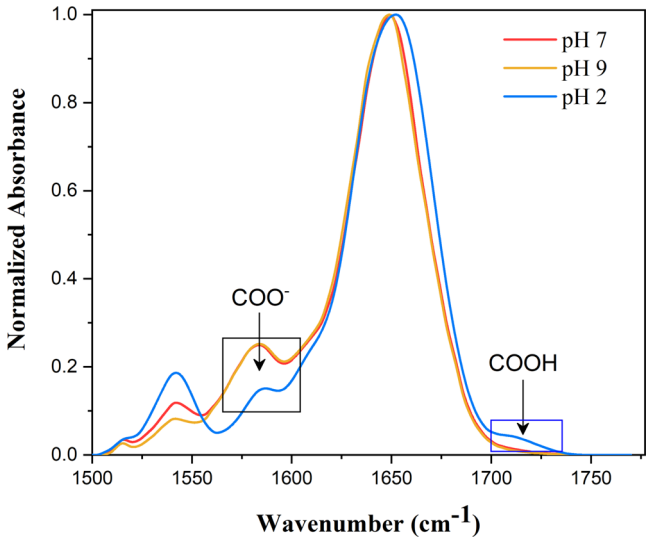

Figure 1. FTIR spectra of lysozyme at pH 7 (red), 9 (yellow), and 2 (blue) in the 1500−1750 cm^{-1} range. All spectra are normalized to the amide-I band peak at ∼1650 cm^{-1}. The black and blue boxes denote carboxylate and carboxylic acid transitions, respectively.

The peak in the 1560−1590 cm^{-1} region of the FTIR spectra at pH 7 and pH 9 (black box, Figure 1) arises due to the C═O stretch of the carboxylate side chains.[13] The carboxylate groups of Asp and Glu have transitions at 1584 and 1567 cm^{-1}, respectively, in D_2O.[5] At pH 2, the peak in the 1700−1730 cm^{-1} region (blue box, Figure 1) can be associated with the C═O stretch of the carboxylic acid side chain of Asp and Glu.[13] A concomitant decrease in the carboxylate absorption (at ∼1580 cm^{-1}) suggests that the side chains get protonated at pH 2. The presence of the peak in the carboxylate region at pH 2 can plausibly be ascribed to the residual carboxylate moieties, indicating that the local protein environment modifies the pK_a values of the individual acidic side chains to varying extents. It is intriguing to comprehend that some of the carboxylate remains deprotonated at pH 2, i.e., at a pH much lower than the solution pK_a values of Asp (3.5) and Glu (4.3). However, an extensive literature search showed indirect (model-based) evidence of Asp pK_a values of ≤2 in lysozyme and other proteins from experimental and theoretical studies.[32−35]

Another peak is observed at ∼1540 cm^{-1} at all pH values. The amide-II peak (predominantly N−H bend) of biomolecules dissolved in H_2O appears at this frequency region (Figure S1 in the Supporting Information). However, the presence of D_2O causes an ∼100 cm^{-1} red shift in this transition due to the H/D exchange of the N−H bond.[36] Therefore, we assign the 1540 cm^{-1} peak to the residual amide-II vibrations arising due to the incomplete deuteration of the backbone NH. Time-dependent FTIR spectra (Figure S2 in the Supporting Information) confirm the H/D exchange process.

https://doi.org/10.1021/acs.biochem.2c00626
Biochemistry 2023, 62, 451−461

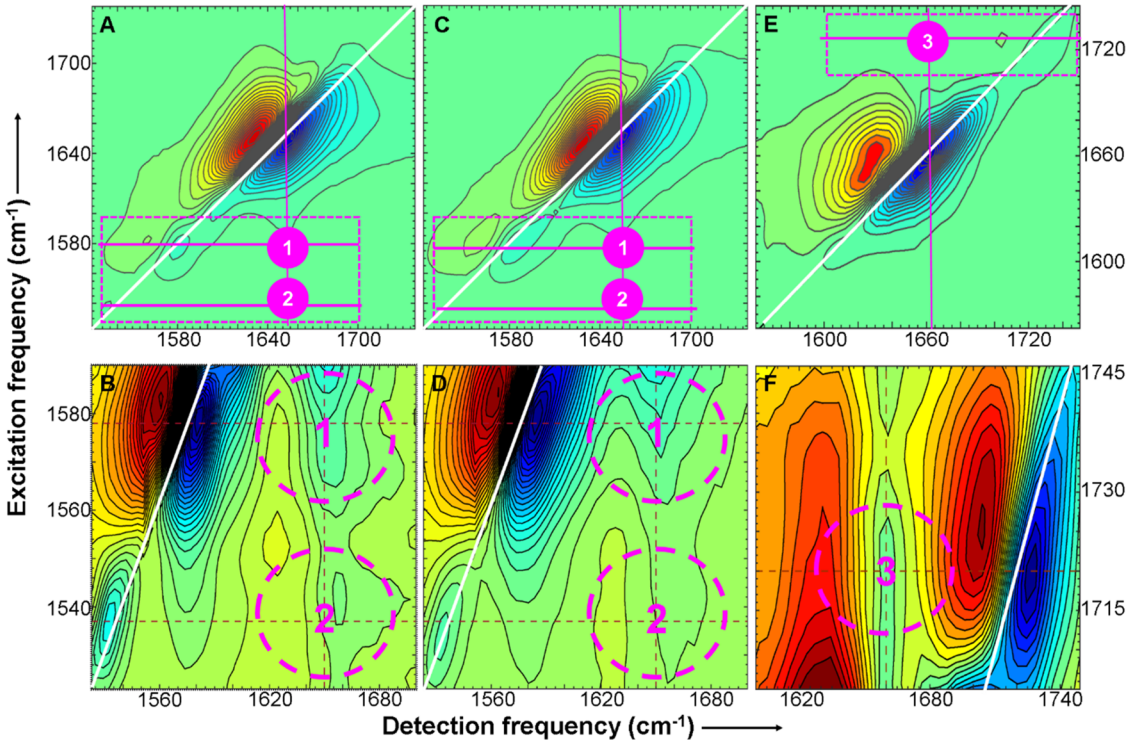

Figure 2. 2D IR spectra of lysozyme at (A) pH 7, (C) pH 9, and (E) pH 2 at T_w = 0 ps. Enlarged views of the spectral window within the dashed rectangular boxes in (A, C, E) are shown in (B, D, F), respectively. The cross-peaks between the COO^- and the amide-I modes are marked as 1 for (B) pH 7 and (D) pH 9; 2 in (B) and (D) represents the cross-peaks between amide-I and amide-II; 3 in (F) represents the cross-peak between amide-I and COOH. The white line represents the diagonal. The vertical and the horizontal magenta lines in top panel are provided to indicate the coupled diagonal peaks that give rise to the cross-peaks. The *y*-axis range for pH 7 and pH 9 is shown on the left, and the *y* axis range for pH 2 is shown on the right.

2D IR Spectra. The 2D IR spectrum of lysozyme at pH 7 (Figure 2A) consists of diagonal peak pairs corresponding to $v = 0 \rightarrow v = 1$ transition (blue) and $v = 1 \rightarrow v = 2$ transition (red) shifted along the detection axis by the diagonal anharmonicity. The amide-I region shows a broad peak pair centered at ~1650 cm^{-1} along the excitation axis. Although an α-helical protein has two overlapping bands in the amide-I region, they cannot be distinguished in the 2D IR spectrum due to their proximity in the transition frequencies and the large inhomogeneous broadening in solution.[37] The carboxylate peak pair is observed along excitation frequency = ~1580 cm^{-1}. An enlarged view of the carboxylate region (Figure 2B) shows cross-peaks (excitation frequency = ~1580 cm^{-1}, detection frequency = ~1650 cm^{-1}) between the carboxylate and the amide-I bands. The cross-peak illustrates that the carboxylate side chains are coupled to the protein backbone. Therefore, any change in the protonation state of the acidic side chains at other pH conditions can plausibly disrupt the side chain−backbone interactions, resulting in a structural change in the protein. Cross-peaks (excitation frequency = ~1540 cm^{-1}, detection frequency = ~1580 cm^{-1}) are also seen between the carboxylates and the residual amide-II band, further emphasizing the side chain−backbone interactions.

At pH 9 (Figure 2C), the amide-I region of the 2D IR spectrum resembles that at pH 7. However, a closer inspection indicates that the carboxylate peak pair becomes more intense, going from pH 7 to pH 9. The increase in the intensity of the carboxylate peak at pH 9 is not observed in FTIR. 2D IR spectroscopy is more sensitive to structural changes than FTIR as 2D IR signals are proportional to the fourth power of the transition dipole strength ($|\vec{\mu}^4|$), unlike $|\vec{\mu}^2|$ in FTIR.[38−40] The carboxylate transition dipole can change if the protein structural modifications alter the solvent exposure. Any change in the solvent exposure would also affect the extent of H/D exchange, resulting in different intensities of the residual amide-II bands, as seen in the FTIR spectra.

Additionally, the intensities of the residual amide-II peaks would affect that of the carboxylate peak due to the spectral overlap. 2D IR spectroscopy allows us to distinguish the overlapping amide-II and carboxylate peaks by spreading the signal into two frequency axes. Similar to our observation at pH 7, carboxylates are also coupled to the amide-I and amide-II modes at pH 9 (Figure 2D). However, slices along the excitation frequency at 1580 cm^{-1} (Figure S3 in the Supporting Information) reveal that the cross-peak's intensity, indicative of side chain−backbone coupling, is weaker at pH 9 than at pH 7. The altered cross-peak intensity with increasing pH indicates a subtle change in the side chain−backbone interactions due to a change in the protein conformation.

At pH 2, a new diagonal peak pair is observed at excitation frequency = ~1720 cm^{-1} (Figure 2E), which arises from the C═O stretch of the carboxylic acid side chains. This peak pair is absent at pH 7 and pH 9. Distinct cross-peaks are observed between the carboxylic acid and the amide-I bands, indicating that the protonated side chains are also coupled to the peptide backbone at pH 2 (Figure 2F). Although both the protonated and deprotonated side chains couple to the backbone, the respective interactions would significantly differ.

In addition, in agreement with the FTIR result, a peak pair is still observed in the carboxylate region at pH 2 (Figure S4 in

https://doi.org/10.1021/acs.biochem.2c00626
Biochemistry 2023, 62, 451−461

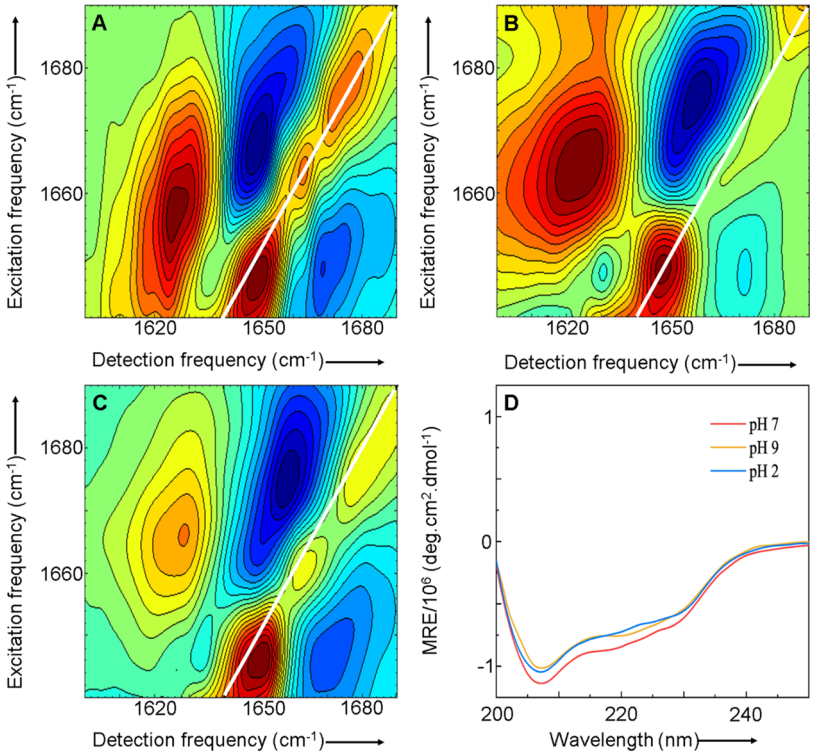

Figure 3. 2D IR polarization difference spectra of lysozyme at pH values of (A) 7, (B) 9, and (C) 2. The difference spectra were obtained by subtracting the parallel polarization spectra data from 3 times the perpendicular polarization spectral data. The white line represents the diagonal. (D) Far-UV CD spectra from 200 to 250 nm at different pH values indicate that the secondary structure is retained for a wide range of pH.

the Supporting Information). This COO^- peak pair is less broadened along the diagonal and considerably less intense than those obtained at higher pH values. Interestingly, the peak at pH 2 appears in the high-frequency region of the carboxylate band obtained at pH 7 and 9. Based on the reported carboxylate frequencies of Asp and Glu, the peak position at pH 2 suggests that the buried carboxylate originates from an Asp.[5] A plausible explanation for the presence of this peak at a wide range of pH values can be that the Asp side chain is less exposed to the solvent at all pH values, and its protonation state is unaffected by the change in pH. Therefore, the side chain remains deprotonated (in the COO^- form) at all three pH values. Residue-specific analysis of each Asp and Glu from MD simulations (discussed later) would allow us to identify the amino acid responsible for the ~1580 cm^{-1} band at pH 2. However, solvent exposure is one of the factors contributing to the energetics of the ionization state of an amino acid residue and thus to the apparent polarizability reported by its pK_a.[41] Many factors, including side chain−side chain interactions, side chain−backbone interactions, presence of buried water molecules, solvent exposure, etc., are capable of altering the polarizability of the acidic side chain.

2D IR spectra reveal pH-dependent changes in the side chain−backbone interactions, which in turn should give rise to the evolution of the protein structure. The distinct change in the protonation states of the side chains indicates a larger conformational change going from pH 7 to pH 2. On the other hand, increasing the pH to 9 only allows subtle structural changes, as seen by the slight change in the cross-peak intensities. Although the carboxylate/carboxylic acid peaks are useful vibrational markers to demonstrate structural evolution as a function of pH, they do not provide information on whether the changes are in the secondary or in the tertiary (side chain packing) structure of the protein. To this end, polarization-dependent 2D IR spectroscopy can determine if lysozyme's secondary structure (primarily α-helix) is retained or lost with changing pH.

An α-helical protein is known to have two coupled modes, A and E_1. Coupling between the two modes gives rise to cross-peaks in the off-diagonal region of the 2D IR spectrum. We exploit the polarization-dependent 2D IR spectra to visualize the cross-peaks. As the transition dipoles of the coupled modes are not parallel, the anisotropy of the diagonal peaks differs from that of the cross-peaks. We have performed polarization-selective 2D IR experiments in the parallel $\langle XXXX \rangle$ and perpendicular $\langle XXYY \rangle$ polarization conditions at the three pH values. The 2D IR difference polarization spectrum ($3\langle XXYY \rangle - \langle XXXX \rangle$) eliminates the diagonal peaks, thereby enhancing the cross-peaks buried underneath the broad amide-I band.[42] Distinct cross-peak pairs are observed at pH 7, pH 9, and pH 2 (Figure 3A−C), respectively.[43] The frequency splitting between the two coupled modes agrees with the previously reported theoretical predictions and 2D IR measurements for α-helical proteins,[5,37,43] thereby indicating that the helical secondary structure is retained in lysozyme at all pH values. Other small peaks observed in Figure 3 can arise from coupling between amino acids that are not part of the helical regions in the lysozyme sequence. These peaks make the difference spectra appear slightly distorted. However, the helical signatures remain intact at neutral, alkaline, and acidic pH. Incomplete cancellation of the diagonal peaks due to slight differences in the laser conditions can also contribute to some of the weak peaks along the diagonal. To validate our findings from 2D IR difference polarization spectra, we have further performed CD spectroscopy on lysozyme at the three different pH conditions. The CD spectra confirm the retention of the

https://doi.org/10.1021/acs.biochem.2c00626
Biochemistry 2023, 62, 451−461

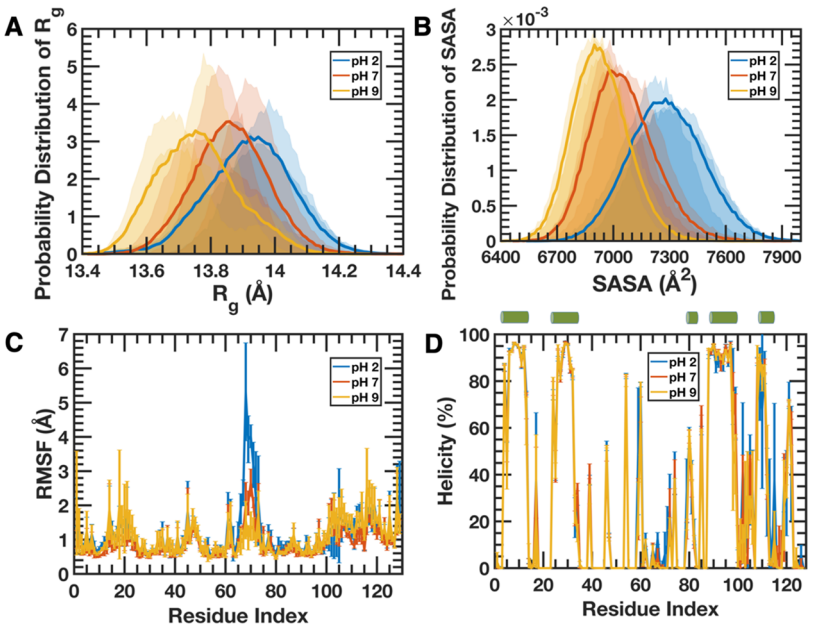

Figure 4. Global and local structural dynamical features. (A) Normalized probability distributions of C_α-based radius of gyration (R_g) of lysozyme under different pH conditions which show the dramatic loss of protein compactness at low pH. The filled areas in the background depict the multiple conformational ensembles obtained from three different simulated trajectories for each of the solution conditions whose amalgamation results in the overall distribution for a specific system. (B) Extent of the variability of the solvent exposure of the entire protein (SASA) as a function of pH exhibits considerably higher solvent exposure of the protein under acidic pH as evident from the normalized probability distribution plots. The background shows the discrete conformational ensembles generated due to the three independent trajectories for a particular system under a specific pH. (C) Sequence-specific time-averaged thermal fluctuations of the protein measured by computing the root-mean-square fluctuation (RMSF) of the C_α atoms. Each of the profiles represents the residue-wise mean RMSF values averaged over the three independent trajectories under a specific solution condition, and the vertical bars represent the standard deviations associated with the RMSF measurement. This shows the existence of one distinct region of lysozyme with greater thermal malleability under acidic pH conditions. (D) Percentage of helicity as a function of residue index averaged over the entire trajectory length. The profile for a given solution condition represents the mean helicity for each residue averaged over the three individual trajectories, and the vertical bars represent the corresponding standard deviations. The green cylinders at the top represent the α-helices present in the native structure of lysozyme having five or more residues. This analysis confirms the overall retainment of the helical characteristic of the protein irrespective of the solution conditions.

helical structure in lysozyme at a wide range of pH. Our experimental results show excellent agreement with previously reported results.[44,45]

The experimental information obtained from the acidic side chains and the amide-I modes in FTIR and 2D IR spectroscopy indicates the following: (1) the helical structure of lysozyme is retained at all pH, (2) the acidic side chains are coupled to the protein backbone, and (3) the pK_a values of the individual Asp and Glu are modified by the protein environment such that at least one Asp remains deprotonated from pH 9 to pH 2. These results hint at pH-sensitive changes in the side chain packing. However, although lysozyme primarily is an α-helical protein, the changes in the other secondary structures cannot be ruled out. MD simulations can provide additional support to the experimental revelations by elucidating the segment-specific and residue-specific changes in various parameters.

MOLECULAR DYNAMICS SIMULATIONS

Characterization of the Simulated Observables. Since three independent trajectories were generated for each of the three solution conditions, we have followed the subsequent representations throughout the manuscript to illustrate the simulated observables comprehensively. The representations include (1) concatenating the global configurational properties and (2) averaging the residue-specific structural features generated from the three trajectories for a specific solution condition.

Global Structural Features. As experimental results suggest that the helical structure is invariant with pH, we have looked at the global structural features of lysozyme to identify the impact of variable pH strength on protein conformation. The near-equilibrium unconstrained simulations, performed to characterize the acquired phase space of the protein in varying pH conditions, depict the preservation of the near-native structural ensembles of the protein at any given pH. The backbone root-mean-square deviation (RMSD) values, calculated with respect to the native protein, remain within the thermal fluctuation limit of the native ensemble (RMSD $\approx$ 1.38 $\pm$ 0.44 Å, Figure S5 in the Supporting Information). The RMSD data indicate a broader range of fluctuations for the ensemble at pH 2 compared to pH 7 and pH 9, suggesting a distinctive conformational feature at pH 2. Moreover, the distinct behavior of the protein at pH 2 emerges when the protein's compactness is considered as an order parameter (C_α R_g, Figure 4A). From the probability distributions of the C_α R_g values, the protein attains a marginally less compact ensemble at pH 2 than at the neutral pH. The relative compactness of the protein is considerably low compared to the alkaline pH. As C_α R_g is a backbone-based order parameter, it might not fully reflect any change in the side chain packing. However, the impact of pH on C_α R_g

https://doi.org/10.1021/acs.biochem.2c00626
Biochemistry 2023, 62, 451−461

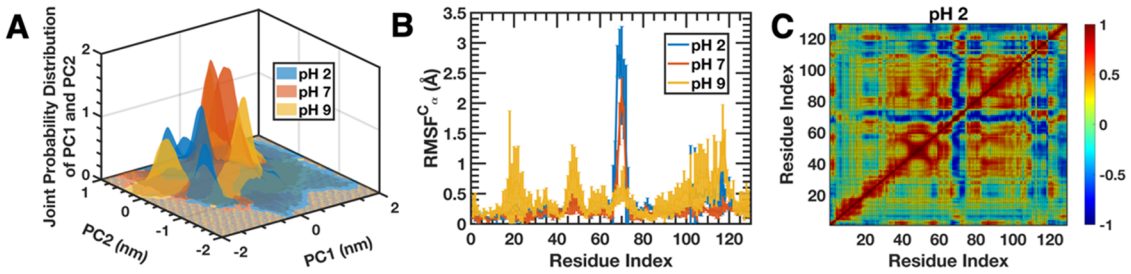

Figure 5. Structural characterization of the protein in terms of intrinsic order parameters. (A) Joint probability distribution of the protein computed by choosing the first two principal components—PC1 and PC2. For a given solution condition, the probability distribution was generated by taking the first two principal component values of all three trajectories. This reconfirms the existence of variability of the lysozyme's global conformational landscape under low-pH conditions as the conformational space is way more diffused under acidic pH compared to the neutral or alkaline ones where the conformational space is much more restricted. (B) Contribution of each residue toward the direction of the most dominant mode of dynamics calculated by estimating the eigenvalues of the C_α atoms of the protein along the direction of PC1. Each profile represents the residue-wise mean RMSF values along the most dominant dynamical mode averaged over the three independent simulations along with the standard deviations associated with every measurement as vertical bars. Interestingly, the observed pattern of contribution changes considerably for a specific region under low-pH conditions, exactly mimicking the observation in Figure 4C. (C) C_α-based dynamical cross-correlation map (DCCM) of the protein under acidic pH condition. The average DCCM obtained by taking the mean of the three DCCMs calculated individually for each of the trajectories at pH 2 was chosen to describe the commonality in the dynamical cross-talk among the residues. The anticorrelated movement of the loop region, which shows higher fluctuations in the RMSF profiles, with respect to the rest of the protein, is evident from the cross-correlation map and thus explains the unique behavior of the protein at the acidic pH condition.

somewhat hints toward a consistent trend, i.e., the lower the pH of the solution, the lower the compactness of the protein.

To include the side chain packing contributions, we have further looked into the extent of exposure (probability distribution of SASA of the protein, Figure 4B) as the order parameter. The backbone-compactness-based hint transforms into an indelible watermark signature in Figure 4B. The protein at pH 2 shows an extensively exposed conformational ensemble than the other two scenarios. The extent of overall solvent exposure of the protein increases with decreasing pH of the solution. The backbone-based RMSD (Figure S5 in the Supporting Information) and C_α R_g reveal that the protein's global structure and the overall fold (backbone) do not drastically change under varying pH conditions within the limits of the simulated timescale. Thus, the backbone-based C_α R_g cannot clearly distinguish the subtle conformational heterogeneity originating from the changes in solution conditions. Since the overall solvent exposure of the protein includes side chain contributions, it also serves as a conclusive identifier of the subtle diversity of the conformational landscapes without any ambiguity.

Local Residue-Specific Characterization. A detailed analysis of the local structural feature has been performed to identify the specific region(s) responsible for the observed heterogeneous response of the protein toward the diversified pH range. The time-averaged residue-wise local fluctuation profiles (C_α RMSF, Figure 4C) convincingly identify one distinct region—residue 65−75—which shows distinctively high local structural deformation at low pH compared to the other two scenarios. This peptide segment forms a loop in the overall structure of lysozyme. As observed in the global compactness and exposure analyses (Figure 4A,B), the change in pH has a highly consistent and systematic impact on the local structural fluctuation of the loop as well—the lower the pH, the higher the flexibility of the loop.

According to the PDB structure, although the protein contains eight helices in its native state, we have only termed a particular segment as a helix if it has five or more residues, leaving us with five helices for the protein. Even though lysozyme is an α-helix-rich protein, the helices retain their structural integrity in a wide range of dynamically changing solution conditions as the distinctive higher RMSF fluctuations do not appear in the helix regions. Time-averaged residue-specific helicity, computed from the unconstrained simulated trajectories (Figure 4D), further validates the presence of the helices at various pH conditions.

Intrinsic Reaction Coordinate. To further substantiate our observation of distinctively different conformations under acidic pH conditions, we have chosen an order parameter (principal component) that is more stringent and inherent than the previously mentioned loosely defined reaction coordinates (e.g., RMSD, R_g, SASA). We have focused on the first two principal components as they dictate ∼65% of the overall dynamics of the protein in all three pH conditions. The joint probability distribution, obtained by considering PC1 and PC2, shows a much broader and more diffused conformational ensemble in the acidic pH than in the other two scenarios. The probability distributions at pH 7 and pH 9 show that high-density peaks appear at specific places of the conformational space (Figure 5A), indicating that the protein retains specific structural features that are not readily interchangeable. On the contrary, in acidic pH, the protein loses out on a few structural identities, and the different species that appear in the conformational space are readily interchangeable as the distribution does not have very sharp peaks and hence, barriers.

The principal component analysis not only helps to identify the global scenario but also has the potential to characterize the local residue-wise features. The fluctuation of PC1 (Figure 5B) shows the extent of fluctuation of each residue in terms of the first mode. Figure 5B reconfirms the conclusion that the maximum fluctuation happens in the residue range 65−75, i.e., the loop region. Interestingly, the consistent impact of lowering pH on the dynamical flexibility of the 11-residue segment of a long loop (Figure 4C) emerges in the dominant-mode-based fluctuation analysis, confirming the robustness of the observation.

Dynamical Cross-Correlation Map. The dynamical cross-correlation maps (DCCMs) of the protein are computed as a function of pH to identify the dynamical heterogeneity

https://doi.org/10.1021/acs.biochem.2c00626
Biochemistry 2023, 62, 451−461

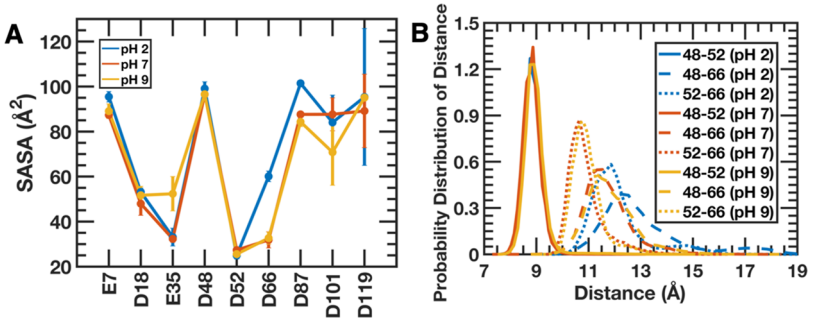

Figure 6. Identification of the key residue(s) in the structural transition of lysozyme. (A) Time-averaged residue-wise solvent exposure calculated for the seven aspartates and two glutamates. Each of the values for a given solution condition was obtained by averaging the three values computed from three independent trajectories. The vertical bars represent the standard deviations associated with each of the measurements. This reconfirms the role of Asp66 as it shows a maximum increment in exposure compared to the neutral or alkaline pH among the buried residues. Interestingly, Asp52, on the contrary, shows the lowest solvent exposure, and the solvent accessibility does not change at all between different solution conditions. (B) Normalized probability distributions of the distances between the C_γ atoms of the three spatially close Asp residues. This shows that the distances increase at lower pH proving the existence of the loop-opening phenomenon. Moreover, the impact of protonation of Asp66 is the most dominant feature as its protonation leads to a much larger increment in inter-residue distance compared to the contribution of the other two aspartates. For each solution condition, the distance distribution represents the combined data of the three independent trajectories.

that differentiates the conformational ensemble of the protein in acidic pH from pH 7 and pH 9 (Figures 5C and S6 in the Supporting Information). These DCCMs have the potential to identify the extent of correlation in movements between different parts of the protein, which might be far apart from each other in terms of covalent bond connectivity but might exist spatially very close. The unique behavior of the protein in acidic pH arises because the N65-L75 loop region, which shows the greatest extent of thermal fluctuations, and hence the maximum degree of dynamical movements in acidic pH (via an 11-residue segment of a long loop), is anticorrelated to the rest of the protein in terms of directed shifts on a three-dimensional (3D) space. Long-range anticorrelated movements lose their dominance in the neutral pH, leading to the lower fluctuation of the specified loop region. As the solution condition changes to alkaline pH, the long-range anticorrelated movement gets reverted into a short-range correlated one. This enormous shift in the directional dynamics of the segmental motions results in the somewhat restricted motion of an otherwise long loop with the lowest magnitude possible compared to the acidic and neutral pH conditions. The direct correlation between the extent of anticorrelated movement and the degree of loop fluctuation can be ascribed to the torque generated by the anticorrelated movements between different protein segments in acidic pH. The torque eventually supplies the energy for the untangling of the protein and leads to segment-specific structural alteration.

Search for the Specific Asp Residue. Since we identified one specific region that acts differently under acidic pH conditions, we further tried to uncover the possibility of finding a particular residue within the region that might be playing the most critical role. Since complementary experimental results have dictated the simulation protocol for changing pH, we focus on all of the aspartate and glutamate residues of the entire protein sequence.

The sequence-dependent exposure analysis of the aspartate and glutamate residues (SASA, Figure 6A) indicates that Asp66 shows the maximum change in solvent exposure going from acidic pH to normal or alkaline pH (~28 Å^2). In addition, Asp52 shows the minimum solvent exposure. The SASA of Asp52 is invariant under different pH conditions. This observation hints at a considerable contribution of the Asp66 toward the extent of fluctuation dynamics of the loop region of lysozyme. This presumption gets further validated by the pair-distance estimation between the C_γ atoms of the three spatially proximal aspartates (Asp48, Asp52, and Asp66) considering these Asp side chains as local structural probes (Figure 6B). This analysis reveals the following: (1) Asp48−Asp52 pair-distance remains comparable at all pH, (2) Asp48−Asp66 and Asp52−Asp66 pair distances show higher values in acidic pH, (3) the change in the pair-distance is considerably higher for Asp48−Asp66 than Asp52−Asp66 at all pH, and (4) the change in pair-distance for a specific pair is much more prominent if one of the residues involved is Asp66. This analysis uncovers that the protonation of Asp66 plays a crucial role in the aggravated dynamics of the loop segment. It is to be noted that Asp66 is the part of the most fluctuating loop region of the protein whose extent of cross-talk with the segmental motions of the rest of the protein dictates the extent of conformational polymorphism of the overall native fold.

Sensitivity Response Profile to the Altered Environment: Side Chain over Backbone. The systematic analysis of the unconstrained simulated trajectories leads to a general idea that the global fold of the protein does not necessarily undergo any significant alteration for a wide range of pH values, as evidenced by the two backbone-based order parameters (RMSD and R_g). The variability in the conformational landscapes originates due to the magnitude of the exposure incorporated by the side chains (SASA). Moreover, the diversified conformational ensembles at pH 2 originate from the fluctuation of the N65-L75 loop region, which in turn gets dictated by the side chain protonation of an Asp66. Therefore, the side chain seems to be the protagonist in the entire act of generating distinguishing expanded conformational ensemble of lysozyme at lower pH. To test the robustness of the above-mentioned logical presumption, we calculated three types of heavy-atom contacts—intra-backbone (BB-BB), intra-side chain (SC-SC), and backbone-side chain (BB-SC). A contact was considered if the distance between a couple of heavy atoms belonging to two different residues falls within a specific distance window.[46] The analysis reveals that the protein loses its contact with decreasing pH majorly due to the lack of interactions involving side chains—be it backbone-side chain (Figure 7B) or intra-side chain (Figure 7C)—the

https://doi.org/10.1021/acs.biochem.2c00626
Biochemistry 2023, 62, 451−461

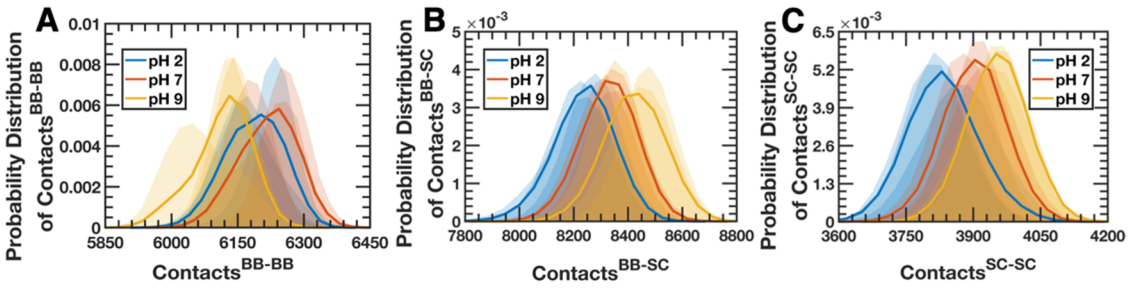

Figure 7. Comparison of the extent of contact formation between the side chains and the backbone of the protein under neutral (red), alkaline (yellow), and acidic (blue) pH conditions represented as normalized probability distributions—(A) intra-backbone, (B) backbone-side chain, and (C) intra-side chain. In each panel, the background-filled areas represent the simulated observables obtained from the three individual trajectories for a specific solution condition with identical color patterns being used for the representation of the overall distribution.

impact is more prominent for the latter case. Interestingly, the consistent and systematic impact of lowering the pH is also evident in the capacity to retain the contacts via side chains, i.e., the lower the pH, the lower the extent of contacts involving side chains. No such trend is observed in the intra-backbone contact profile comparison (Figure 7A). This observation directs us to a conclusion that the protein does not necessarily change its fold at pH 2 but practically gets a bit swollen up.

Comparison between Experiments and Simulations. MD simulations provide detailed molecular-level predictions of the pH-induced structural evolution of lysozyme. However, the quality of any prediction based on molecular dynamics results will strongly depend on the validity of underlying physical assumptions. To this end, comparing multiple computational predictions with experimental results provides a robust foundation. First, both 2D IR experiments and MD simulations demonstrate that the lysozyme helices maintain their structural integrity for a wide range of pH, indicating that the secondary structure of the protein is primarily unchanged from pH 2 to 9. Second, the decrease in the 2D IR cross-peak intensity between the carboxylate and the amide-I peaks hinted at a subtle change in the protein conformation from pH 7 to 9. The simulations reveal that the protein becomes more compact at pH 9. However, a less significant change in the SASA agrees with the subtle change predicted by the 2D IR spectra. Third, the primary structural change of lysozyme is observed at pH 2 in both experiments and simulations. FTIR spectra indicate a slight broadening and a concomitant blue shift of the amide-I band. This result can be explained by a less compact protein structure at the acidic pH, resulting in a more extensive sampling of the conformational space, as indicated by the MD simulation. Fourth, the residual diagonal peak pair ∼1580 cm^{-1}, observed at pH 2, indicated that at least one of the acidic side chains is buried in the protein core and stays in the deprotonated state. In addition, the transition frequency suggested that the residue is an Asp. Simulations predicted that the solvent exposure of Asp52 is minimal and does not vary with solution pH. Moreover, Asp52 is found to be deprotonated under physiological conditions.

■ CONCLUSIONS

In this work, we have combined experimental and computational methods to understand the subtle changes in the lysozyme structure as a function of pH. We show that multiple vibrational markers can provide complementary results about the changes in the protein conformations and the interactions between the backbone and the side chains of the protein. Previously, 2D IR spectroscopy has been extensively used to distinguish the protein conformations based on the distinct signatures of the amide-I peaks for different secondary structures. However, despite the importance of side chain−backbone interactions, 2D IR reports on the side chain C═O are rare. Our experimental results indicate that although the helical structure is retained from pH 2 to 9, the change in pH alters the protonation states of the acidic side chains, affecting the protein conformations. The change is found to be maximum at the acidic pH.

We have evaluated the pH-dependent global structural features (RMSD, SASA, and R_g) of lysozyme from MD simulations. We find that the protein attains a less compact structure as the pH of the solution is lowered, which was further validated by the increase in the SASA. However, RMSD data indicated that the secondary structure of the protein is retained at all pH values. Despite the helical structure at a wide range of pH, residue-specific characterization identified one distinct loop region (residues 65−75) undergoing local structural deformation at low pH. The principal component analysis supported our residue-specific predictions. Further, Asp66 was found to be affected upon protonation/deprotonation, while the minimum effect of pH was observed on Asp52. These results further demonstrate that the pK_a of Asp and Glu depends on the local environment in the protein.

In a nutshell, we have compared our experimental results with those predicted from simulations on multiple fronts. The excellent agreement of the simulation results validates the robustness of our predictions on the residue-specific understanding. Although this work focuses on lysozyme, the combined 2D IR/MD simulations approach should generally apply to any protein. The use of complementary vibrational markers increases the scope of comparison with the simulation results, thereby benchmarking the robustness of the simulations. As any change in the solution pH affects the acidic side chain to different extents, the development of constant pH MD simulations is crucial for obtaining a deep insight into small structural changes. This work emphasizes that a combination of 2D IR experiments and MD simulations can provide an effective and novel route to obtaining a molecular understanding of these structural changes in proteins.

■ ASSOCIATED CONTENT

Supporting Information

The Supporting Information is available free of charge at https://pubs.acs.org/doi/10.1021/acs.biochem.2c00626.

https://doi.org/10.1021/acs.biochem.2c00626
Biochemistry 2023, 62, 451−461

Additional FTIR and 2D IR spectra and additional graphs from MD simulations (PDF)

AUTHOR INFORMATION

Corresponding Authors

Atanu Das − *Physical and Materials Chemistry Division, CSIR-National Chemical Laboratory, Pune 411008, India; Academy of Scientific and Innovative Research (AcSIR), Ghaziabad 201002, India;* orcid.org/0000-0003-4994-0469; Email: as.das@ncl.res.in

Sayan Bagchi − *Physical and Materials Chemistry Division, CSIR-National Chemical Laboratory, Pune 411008, India; Academy of Scientific and Innovative Research (AcSIR), Ghaziabad 201002, India;* orcid.org/0000-0001-6932-3113; Email: s.bagchi@ncl.res.in

Authors

Shivshankar Kore − *Physical and Materials Chemistry Division, CSIR-National Chemical Laboratory, Pune 411008, India; Academy of Scientific and Innovative Research (AcSIR), Ghaziabad 201002, India;* orcid.org/0000-0001-5728-8197

Samadhan H. Deshmukh − *Physical and Materials Chemistry Division, CSIR-National Chemical Laboratory, Pune 411008, India; Academy of Scientific and Innovative Research (AcSIR), Ghaziabad 201002, India;* orcid.org/0000-0002-0326-6125

Sushil S. Sakpal − *Physical and Materials Chemistry Division, CSIR-National Chemical Laboratory, Pune 411008, India; Academy of Scientific and Innovative Research (AcSIR), Ghaziabad 201002, India*

Srijan Chatterjee − *Physical and Materials Chemistry Division, CSIR-National Chemical Laboratory, Pune 411008, India; Academy of Scientific and Innovative Research (AcSIR), Ghaziabad 201002, India;* orcid.org/0000-0001-9701-4158

Complete contact information is available at: https://pubs.acs.org/10.1021/acs.biochem.2c00626

Notes

The authors declare no competing financial interest.

ACKNOWLEDGMENTS

S.B. acknowledges CSIR-NCL and SERB, India (EMR/2016/000576), for financial support. The authors acknowledge the computational facilities at CSIR-NCL. They also acknowledge National Supercomputing Mission (NSM) for providing computing resources of "PARAM Brahma" at IISER Pune, which is implemented by C-DAC and supported by the Ministry of Electronics and Information Technology (MeitY) and Department of Science and Technology (DST), Government of India. Additional computing facilities from CSIR Fourth Paradigm Institute are gratefully acknowledged. Central CD facilities at CSIR-NCL are also acknowledged. The authors acknowledge Arnab Mukherjee (IISER Pune) and Santosh Kumar Jha (CSIR-NCL) for insightful scientific discussions. S.K. acknowledges DBT, S.H.D. acknowledges CSIR, and S.S.S. acknowledges UGC for research fellowships.

REFERENCES

(1) Krimm, S.; Bandekar, J. Vibrational Spectroscopy and Conformation of Peptides, Polypeptides, and Proteins. In *Advances in Protein Chemistry Volume*; Anfinsen, C. B.; Edsall, J. T.; Richards, F. M., Eds.; Academic Press, 1986; Vol. *38*, pp 181−364.

(2) Torii, H.; Tasumi, M. Application of the three-dimensional doorway-state theory to analyses of the amide-I infrared bands of globular proteins. *J. Chem. Phys.* **1992**, *97*, 92−98.

(3) Torii, H.; Tasumi, M. Model calculations on the amide-I infrared bands of globular proteins. *J. Chem. Phys.* **1992**, *96*, 3379−3387.

(4) Choi, J.-H.; Ham, S.; Cho, M. Inter-peptide interaction and delocalization of amide I vibrational excitons in myoglobin and flavodoxin. *J. Chem. Phys.* **2002**, *117*, 6821−6832.

(5) Barth, A.; Zscherp, C. What vibrations tell about proteins. *Q. Rev. Biophys.* **2002**, *35*, 369−430.

(6) Surewicz, W. K.; Mantsch, H. H.; Chapman, D. Determination of protein secondary structure by Fourier transform infrared spectroscopy: a critical assessment. *Biochemistry* **1993**, *32*, 389−394.

(7) Demirdöven, N.; Cheatum, C. M.; Chung, H. S.; Khalil, M.; Knoester, J.; Tokmakoff, A. Two-dimensional infrared spectroscopy of antiparallel β-sheet secondary structure. *J. Am. Chem. Soc.* **2004**, *126*, 7981−7990.

(8) Zanni, M. T.; Gnanakaran, S.; Stenger, J.; Hochstrasser, R. M. Heterodyned two-dimensional infrared spectroscopy of solvent-dependent conformations of acetylproline-NH2. *J. Phys. Chem. B* **2001**, *105*, 6520−6535.

(9) Woutersen, S.; Hamm, P. Nonlinear two-dimensional vibrational spectroscopy of peptides. *J. Phys.: Condens. Matter* **2002**, *14*, R1035−R1062.

(10) Khalil, M.; Demirdöven, N.; Tokmakoff, A. Coherent 2D IR spectroscopy: Molecular structure and dynamics in solution. *J. Phys. Chem. A* **2003**, *107*, 5258−5279.

(11) Grimsley, G. R.; Scholtz, J. M.; Pace, C. N. A summary of the measured pK values of the ionizable groups in folded proteins. *Protein Sci.* **2009**, *18*, 247−251.

(12) Kukić, P.; Farrell, D.; Søndergaard, C. R.; Bjarnadottir, U.; Bradley, J.; Pollastri, G.; Nielsen, J. E. Improving the analysis of NMR spectra tracking pH-induced conformational changes: Removing artefacts of the electric field on the NMR chemical shift. *Proteins: Struct., Funct., Bioinf.* **2010**, *78*, 971−984.

(13) Bagchi, S.; Falvo, C.; Mukamel, S.; Hochstrasser, R. M. 2D-IR experiments and simulations of the coupling between amide-I and ionizable side chains in proteins: application to the Villin headpiece. *J. Phys. Chem. B* **2009**, *113*, 11260−11273.

(14) Harris, T. K.; Turner, G. J. Structural basis of perturbed pKa values of catalytic groups in enzyme active sites. *IUBMB Life* **2002**, *53*, 85−98.

(15) Cabaniss, S. E.; McVey, I. F. Aqueous infrared carboxylate absorbances: aliphatic monocarboxylates. *Spectrochim. Acta, Part A* **1995**, *51*, 2385−2395.

(16) Cabaniss, S.; Leenheer, J.; McVey, I. Aqueous infrared carboxylate absorbances: aliphatic di-acids. *Spectrochim. Acta, Part A* **1998**, *54*, 449−458.

(17) Humbert, B.; Alnot, M.; Quilès, F. Infrared and Raman spectroscopical studies of salicylic and salicylate derivatives in aqueous solution. *Spectrochim. Acta, Part A* **1998**, *54*, 465−476.

(18) Binev, I. G.; Vassileva-Boyadjieva, P.; Binev, Y. I. Experimental and ab initio MO studies on the IR spectra and structure of 4-hydroxyacetanilide (paracetamol), its oxyanion and dianion. *J. Mol. Struct.* **1998**, *447*, 235−246.

(19) Keresztury, G.; István, K.; Sundius, T. Applicability of the SQM force field method to the vibrational spectra of sodium acetate. *J. Phys. Chem. A* **2005**, *109*, 7938−7945.

(20) Max, J.-J.; Chapados, C. Infrared spectroscopy of aqueous carboxylic acids: comparison between different acids and their salts. *J. Phys. Chem. A* **2004**, *108*, 3324−3337.

(21) Fink, A. L.; Calciano, L. J.; Goto, Y.; Kurotsu, T.; Palleros, D. R. Classification of Acid Denaturation of Proteins: Intermediates and Unfolded States. *Biochemistry* **1994**, *33*, 12504−12511.

(22) Mongan, J.; Case, D. A.; McCammon, J. A. Constant pH molecular dynamics in generalized Born implicit solvent. *J. Comput. Chem.* **2004**, *25*, 2038−2048.

(23) Chatterjee, S.; Ghosh, D.; Haldar, T.; Deb, P.; Sakpal, S. S.; Deshmukh, S. H.; Kashid, S. M.; Bagchi, S. Hydrocarbon Chain-Length Dependence of Solvation Dynamics in Alcohol-Based Deep Eutectic Solvents: A Two-Dimensional Infrared Spectroscopic Investigation. *J. Phys. Chem. B* **2019**, *123*, 9355−9363.
(24) Pronk, S.; Páll, S.; Schulz, R.; Larsson, P.; Bjelkmar, P.; Apostolov, R.; Shirts, M. R.; Smith, J. C.; Kasson, P. M.; van der Spoel, D.; Hess, B.; Lindahl, E. GROMACS 4.5: a high-throughput and highly parallel open source molecular simulation toolkit. *Bioinformatics* **2013**, *29*, 845−854.
(25) Bjelkmar, P.; Larsson, P.; Cuendet, M. A.; Hess, B.; Lindahl, E. Implementation of the CHARMM Force Field in GROMACS: Analysis of Protein Stability Effects from Correction Maps, Virtual Interaction Sites, and Water Models. *J. Chem. Theory Comput.* **2010**, *6*, 459−466.
(26) Artymiuk, P. J.; Blake, C. C. F.; Rice, D. W.; Wilson, K. S. The Structures of the Monoclinic and Orthorhombic Forms of Hen Egg-White Lysozyme at 6 Angstroms Resolution. *Acta Crystallogr., Sect. B: Struct. Crystallogr. Cryst. Chem.* **1981**, *38*, 778−783.
(27) Demchuk, E.; Wade, R. C. Improving the Continuum Dielectric Approach to Calculating pKas of Ionizable Groups in Proteins. *J. Phys. Chem. A* **1996**, *100*, 17373−17387.
(28) Bussi, G.; Donadio, D.; Parrinello, M. Canonical sampling through velocity rescaling. *J. Chem. Phys.* **2007**, *126*, No. 014101.
(29) Parrinello, M.; Rahman, A. Polymorphic transitions in single crystals: A new molecular dynamics method. *J. Appl. Phys.* **1981**, *52*, 7182−7190.
(30) Hess, B. P-LINCS: A Parallel Linear Constraint Solver for Molecular Simulation. *J. Chem. Theory Comput.* **2008**, *4*, 116−122.
(31) Darden, T.; York, D.; Pedersen, L. Particle mesh Ewald: An N·log(N) method for Ewald sums in large systems. *J. Chem. Phys.* **1993**, *98*, 10089−10092.
(32) Sakakibara, R.; Hamaguch, K. Structure of Lysozyme: XVI. Acid-Base Titration of Lysozyme. *J. Biochem.* **1968**, *64*, 613−618.
(33) Tanford, C.; Roxby, R. Interpretation of protein titration curves. Application to lysozyme. *Biochemistry* **1972**, *11*, 2192−2198.
(34) Pfeil, W.; Privalov, P. L. Thermodynamic investigations of proteins: I. Standard functions for proteins with lysozyme as an example. *Biophys. Chem.* **1976**, *4*, 23−32.
(35) Kuramitsu, S.; Hamaguchi, K. Analysis of the Acid-Base Titration Curve of Hen Lysozyme1. *J. Biochem.* **1980**, *87*, 1215−1219.
(36) Barth, A. Infrared spectroscopy of proteins. *Biochim. Biophys. Acta, Bioenerg.* **2007**, *1767*, 1073−1101.
(37) Huerta-Viga, A.; Woutersen, S. Protein denaturation with guanidinium: a 2D-IR study. *J. Phys. Chem. Lett.* **2013**, *4*, 3397−3401.
(38) Dunkelberger, E. B.; Grechko, M.; Zanni, M. T. Transition Dipoles from 1D and 2D Infrared Spectroscopy Help Reveal the Secondary Structures of Proteins: Application to Amyloids. *J. Phys. Chem. B* **2015**, *119*, 14065−14075.
(39) Kim, Y. S.; Hochstrasser, R. M. Chemical exchange 2D IR of hydrogen-bond making and breaking. *Proc. Natl. Acad. Sci. U.S.A.* **2005**, *102*, 11185−11190.
(40) Kashid, S. M.; Singh, R. K.; Kwon, H.; Kim, Y. S.; Mukherjee, A.; Bagchi, S. Arresting an Unusual Amide Tautomer Using Divalent Cations. *J. Phys. Chem. B* **2019**, *123*, 8419−8424.
(41) Fitch, C. A.; Karp, D. A.; Lee, K. K.; Stites, W. E.; Lattman, E. E.; García-Moreno, E. B. Experimental pKa Values of Buried Residues: Analysis with Continuum Methods and Role of Water Penetration. *Biophys. J.* **2002**, *82*, 3289−3304.
(42) Hamm, P.; Zanni, M. *Concepts and Methods of 2D Infrared Spectroscopy*; Cambridge University Press, 2011.
(43) Woutersen, S.; Hamm, P. Time-resolved two-dimensional vibrational spectroscopy of a short α-helix in water. *J. Chem. Phys.* **2001**, *115*, 7737−7743.
(44) Jha, I.; Rani, A.; Venkatesu, P. Sustained Stability and Activity of Lysozyme in Choline Chloride against pH Induced Denaturation. *ACS Sustainable Chem. Eng.* **2017**, *5*, 8344−8355.
(45) Babu, K. R.; Bhakuni, V. Ionic-Strength-Dependent Transition of Hen Egg-White Lysozyme at Low PH to a Compact State and its Aggregation on Thermal Denaturation. *Eur. J. Biochem.* **1997**, *245*, 781−789.
(46) Best, R. B.; Hummer, G.; Eaton, W. A. Native contacts determine protein folding mechanisms in atomistic simulations. *Proc. Natl. Acad. Sci. U.S.A.* **2013**, *110*, 17874−17879.

https://doi.org/10.1021/acs.biochem.2c00626
Biochemistry 2023, 62, 451−461